International Forum on Aeroelasticity and Structural Dynamics
IFASD 2019
9-13 June 2019, Savannah, Georgia, USA

DESIGN AND WIND TUNNEL TEST OF AN ACTIVELY CONTROLLED FLEXIBLE WING

Wolf R. Krüger[1*], Johannes K.S. Dillinger[1], Yasser M. Meddaikar[1], Jannis Lübker[1], Martin Tang[1], Tobias Meier[1], Marc Böswald[1], Keith Soal[1], Manuel Pusch[2], Thiemo Kier[2]

[1] Institute of Aeroelasticity, German Aerospace Center (DLR),
37073 Göttingen, Germany

[*]Wolf.Krueger@DLR.de

[2] Institute of System Dynamics and Control, German Aerospace Center (DLR),
82234 Weßling, Germany

Kewords: Wind tunnel testing, aeroelastic model, load control

Abstract: The reduction of flight loads has the potential to reduce structural mass in wing design and to improve passenger comfort. In the DLR project KonTeKst, an actively controlled wing was designed, manufactured and tested in a wind tunnel experiment. The motivation of the activity was to validate methods for the design of combined passive and active load alleviation techniques, including aeroelastic tailoring and active load control. In addition, the experimental activities provided an opportunity to improve and validate modal identification techniques. The wind tunnel model is a flexible composite wing of 1.6 meter (half-) span, with three flaps used for load control. The control design uses H_2 optimal blending techniques for input and output. The control strategy is capable of accounting for failure of one flap without critically losing performance. The wind tunnel experiment was performed in a wind tunnel with a maximum speed of 50 m/s. The paper will give an overview of the numerical design activities for wing and load control, of wing design and manufacturing, including the selection and installation of sensors and actuators, and of the wind tunnel set up including the actuation of the wing, data acquisition and online analysis, as well as selected results.

1 INTRODUCTION

1.1 Background

The work presented in this paper is part of the DLR *KonTeKst* (Configurations and Technologies for Short Range Aircraft) project which focusses on the development and analysis of configurations and technologies for emission and noise reduction for short range aircraft. Within the project, methods for load analysis and load reduction are developed. The design and testing of the active wing was a key activity to validate the design and analysis processes of the two partners of the work package, the DLR Institute of Aeroelasticity in Göttingen, Germany, and the DLR Institute of System Dynamics and Control in Oberpfaffenhofen, Germany.

The Institute of Aeroelasticity has a long standing background in the design of wings for passive load alleviation, often called aeroelastic tailoring [1], as well as in comprehensive load analysis [2], structural identification [3] and aeroelastic wind tunnel testing at subsonic

and transonic speeds [4]. The Institute of System Dynamics and Control is also active in load analysis [5] and has wide-ranging developments in flight control [6] and load control [7]. Summarized, the experiment thus had the following goals:

- Extension of the aeroservoelastic design and testing capabilities of DLR, especially
- Validation of the aeroelastic tailoring process of the DLR Institute of Aeroelasticity,
- Validation of the load control design strategy of the DLR Institute of System Dynamics and Control,
- Development of online structural identification methods,
- Improvement of real time control of wind tunnel models.

1.2 Definition of the experiment

The design and testing of the actively controlled wing comprised the following activities – first, a flexible composite wing of 1.6 meter (half-) span, with three flaps used for load control, was designed using the DLR aeroelastic tailoring process. In parallel, the control design using H_2 optimal blending techniques for input and output was performed. The wind tunnel model was manufactured and equipped with sensors. Actuators for the control surfaces were selected and qualified. The structural dynamic properties of the model were identified in a vibration test. The wind tunnel experiment was performed in a wind tunnel capable of reaching 60 m/s, however, it was decided to perform the main part of the tests around 40 m/s. To simulate gust input, the root of the wing was subject to pitch excitations, see Figure 1, the flow in turn exciting deflections of the wing, mainly vertical to its planform. The controller had the objective to minimize root bending moment, by minimizing the vertical acceleration.

In the following sections, the steps are explained closer. However, as this paper is intended to give an overview of the activities, some topics are explained in more detail in further publications cited in the respective sections of this paper.

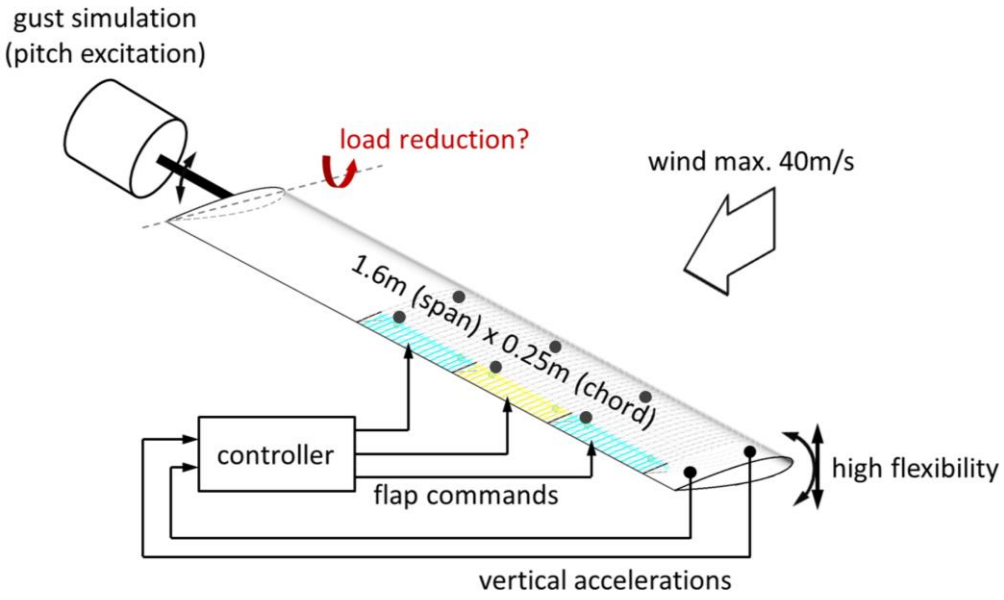

Figure 1: Overview of experiment

2 MODEL DESIGN AND COMPONENT TESTING

2.1 Model Design

The first step in the wing design for the load control experiment was the selection of a suitable layout. Previous experiments in the Göttingen SWG wind tunnel aimed at the investigation of passive wings undergoing large deflections and had been performed with unswept [8] and forward swept wings [9].

The objective of the wing design task for the current investigation was to cover the entire process from design and optimization, over manufacturing and instrumentation to testing. In order to reduce modeling uncertainties, and to be able to focus on an adequate finite element and aerodynamic representation, a rather simple wing layout was chosen over a complex wing shape, see Figure 2. The wing was equipped with three flaps to allow freedom for control design. As the main goal was to perform gust control, a symmetric airfoil seemed to be best for validation, thus a NACA 0015 airfoil was used, thick enough to contain sensors and flap actuators. The chord of the untampered wing was 0.25 m, resulting in a reference area of 0.8 m^2 and an aspect ratio of 12.8.

Glass fiber composite was used for the wing skin, as it had shown in previous projects (see again [9]) to result in relatively flexible wings with low natural frequencies, preferable for the low speed wind tunnel.

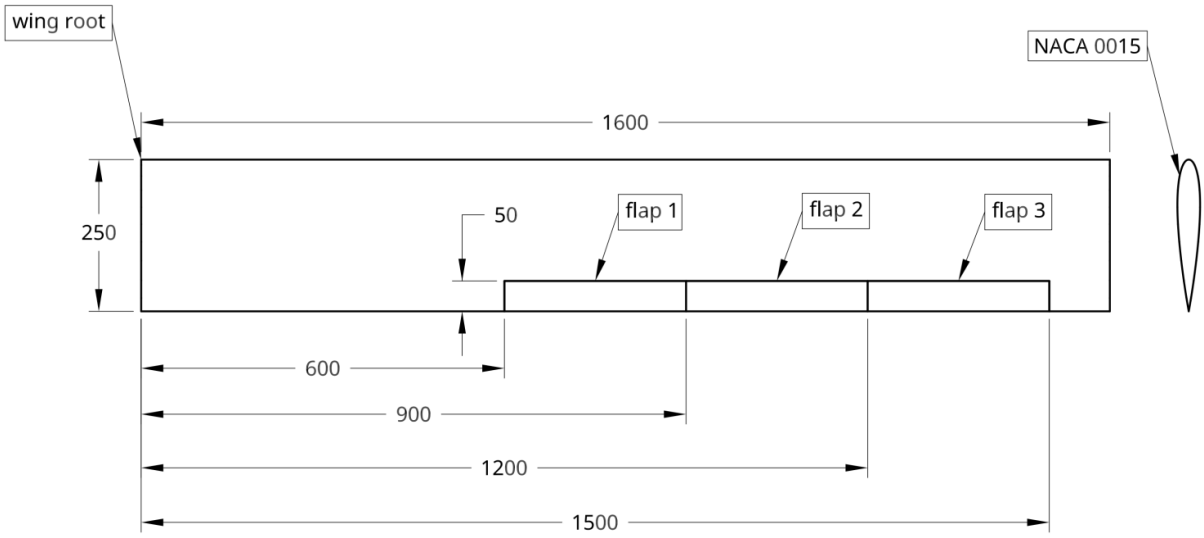

Figure 2: Wing layout

The finite element model of the wing is shown in Figure 3. The aeroelastic tailoring process works in two steps, see also [1] and [10]. First, a suitable stiffness distribution is determined for an objective function of choice. For the current wing design, several objective functions were investigated in detail, and a function maximizing aileron effectiveness was finally employed. Second, blended stacking sequences for the composite material are optimized, eventually leading to layup tables directly suitable for the manufacturing process.

A more detailed description of the wing design process can be found in the paper by Dillinger et al also presented at IFASD 2019 [11].

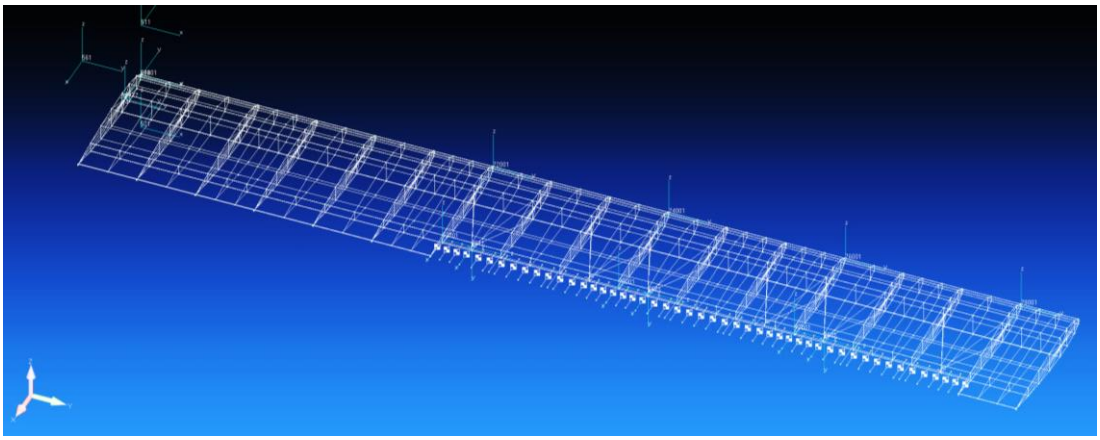

Figure 3: Finite element model of wing with flaps

2.2 Controller Design

The objective of the load control approach investigated in the experiment was gust control. To provide input for the control scheme, the wing was equipped with eight accelerometers, measuring vertical acceleration, arranged in pairs at locations matching the flap boundaries at 0.6 m, 0.9 m, 1.2 m and 1.5 m span.

For active gust load alleviation, the goal is to reduce the wing root bending moment by a coordinated deflection of the three trailing edge flaps based on the eight vertical acceleration measurements. Carrying out a modal decomposition on the state space model of the flexible wing, the contribution of each aeroelastic mode to the wing root bending moment is determined using the $\mathcal{H}_2$ norm. As expected, the lightly damped wing bending modes have the largest contributions, where only the first one is within the actuator bandwidth. Hence, a gust load alleviation controller is designed which increases the damping of the first wing bending mode using the modal control approach from [7]. The control approach suggests isolating the target mode by blending control inputs and measurement outputs in an $\mathcal{H}_2$-optimal way in order to enable a subsequent single-input single-output (SISO) controller design. In other words, the measurement outputs are weighted and summed up such that the resulting scalar signal best represents the response of target mode. Similarly, the control commands computed by the SISO controller are distributed to the available flaps in a way that the target mode is damped efficiently without exciting other modes. The resulting closed-loop interconnection is depicted in Figure 4.

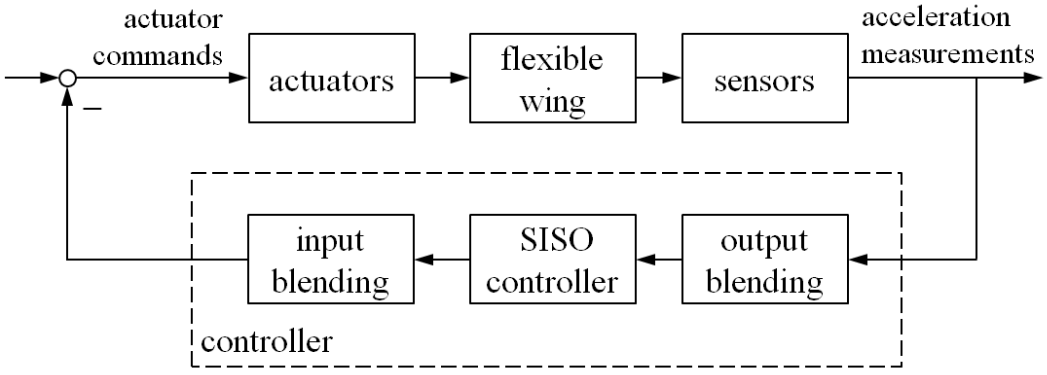

Figure 4: Control-loop interconnection

As the dynamics of the flexible wing vary with the true airspeed V_{TAS}, a scheduling of the gust load alleviation controller is recommended. To that end, the SISO controller is gain-scheduled with V_{TAS} while the input and output blendings are kept constant since the shape of the target mode they depend on remains almost constant within the considered airspeed range. Using a proportional-integral (PI) SISO controller, the corresponding gains are tuned at $VTAS$ = 20, 30 and 40m/s such that gain and phase margins of at least 6dB and 45° are ensured and no actuator saturation occurs for the worst-case harmonic excitation causing ±10cm wing tip deflection. In between the considered design points, the controller gains are linearly interpolated.

In order to handle actuator saturation, a control allocation scheme is implemented which adapts the blending of the control inputs accordingly. To that end, a quadratic program is solved at each time sample, which aims to minimize the additional control effort required to keep the current control commands within actuator limitations [12]. To guarantee a feasible solution of the quadratic program, a slacking variable is introduced, which can be seen as a controller performance degradation in case the control command of the SISO controller cannot be realized. The implemented control allocation scheme considers both deflection and deflection rate limitations and is also used to handle actuator jamming by adapting the actuator limitations accordingly. For more details on modal controller design and control allocation see [12] and [13], respectively.

2.3 Manufacturing of Wing, Actuator and Sensor Installation

The assessment and validation of the DLR in-house aeroelastic tailoring process was one of the main drivers of the experiment. Thus, the wing was manufactured such that a close correlation to the finite element model could be maintained. Another important aspect was the instrumentation of the wing with sensors and actuators. The manufacturing process consisted of the following steps - first, the upper and lower wing skins were manufactured in CNC milled molds, then the sensors were installed, including fiber optical sensors for strain measurements, twelve accelerometers (ten vertical, two in-plane), six three-axes accelerometers (acting as inclinometers), four strain gauges, and potentiometers in the flap hinge lines, see Figure 5. Finally, the wing was closed, and the flap actuators were installed from outside. During the experiment, the total force and moments around all axes at the wing root were additionally measured by a piezo-electric wind tunnel balance.

Figure 5: Open wing after sensor installation

The flap drives of the wing are a combination of commercially available and specially designed components. The actuator mechanisms consisting of servo, push-pull rods and trailing edge control surface have been designed for active gust load alleviation. Of special interest for the load control experiment is the required actuation frequency together with the necessary amplitude. As the goal was to increase the damping of the fundamental wing bending mode, an actuation frequency of 20 Hz at a control surface deflection of ±10 degrees was specified. Free play in the drive mechanism should remain as small as possible since it greatly affects the performance of the controller. The availability of a dynamic substitute model of the actuator is a prerequisite for control law design. Static properties of servos are given by the manufacturer, but the actuator dynamics are in general unknown and have to be determined experimentally. Regan [14] provides an extensive survey on servos for the flying wing aircraft mAEWing2. Based on this overview and on own research, two types of servos, the Futaba BLS471SV and the MKS HBL990 brushless digital servo, have been chosen as candidates for this loads alleviation experiment.

Servo actuators are typically characterized by maximum torque and maximum rate of rotation without any operating load. However, the dynamic behavior of the servo depends on the excitation frequency, deflection amplitude, and most likely, also on the inertia load to be actuated. It is thus necessary to identify an appropriate dynamic model to be included in the overall simulation model for control law design. For this purpose, a specific servo test rig was designed, see Figure 6. The test rig emulates the inertia and the mechanical gain of the drive mechanism for obtaining the actuator transfer functions. The rig consists of a 3D printed wing section; a composite control surface has been used to find the best solution for mechanical integration of the servo, the drive mechanism, the control surface hinge bearings and sensors for the angular deflection of the control surface.

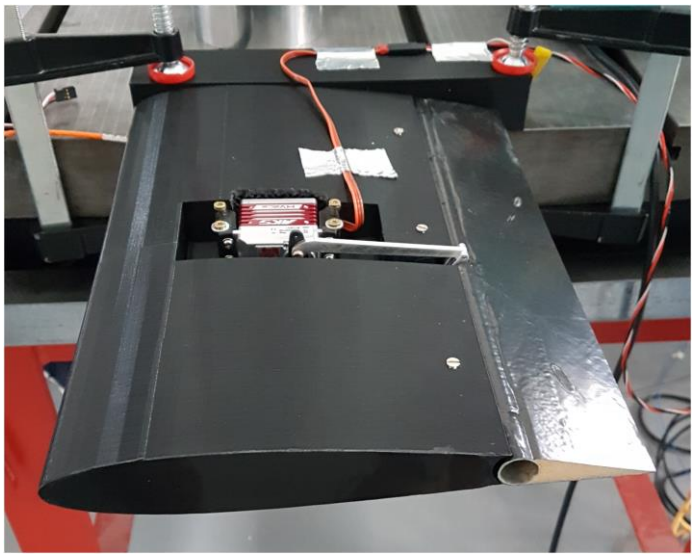

Figure 6: Actuator test in dummy wing section

On this test-rig, the transfer functions of the servo-actuators were identified using sine sweep excitations at a discrete number of different flap amplitudes. The servo comes as a motor driven by a built-in real-time controller, which for the experiment, has been regarded as a ‘black box’. The controller receives analog command signals as inputs and translates them in real-time into Pulse-Width Modulated (PWM) drive signals sent to the servos. For the identification of the transfer function, the analog command signal for the angular deflection of the servo and the actual angular deflection of the control surface are measured. The actual deflection is determined with a potentiometer which is mounted at the hinge. Using these two signals, the transfer function is computed in order to estimate the bandwidth of the actuator.

The frequency response for the MKS HBL990 is shown in Figure 7. It can be seen that an amplitude of 5° at 20 Hz is in the linear range of the actuator. For higher commanded amplitudes, a loss of performance is visible.

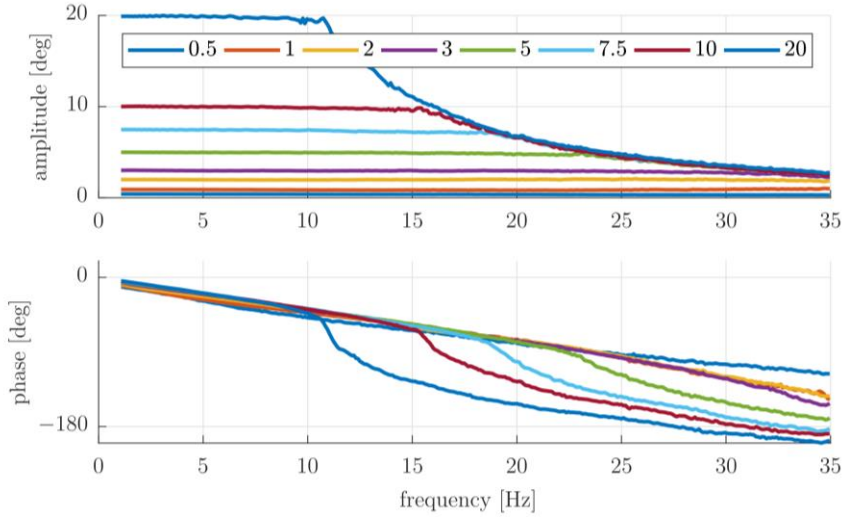

Figure 7: Frequency response from commanded flap deflection to measured flap deflection for different amplitudes

The actuator free play, maximum velocity, and delay have been assessed as well. Based on the results of the tests, the MKS HBL990 was chosen to drive the flaps. After implementation of the servos into the final wing model, a subsequent test was performed to validate the data from the test-rig and to validate the numerical model. These tests provided also the transfer functions from the actuator to the built-in accelerometers. The obtained transfer functions are a fundamental basis for the modal controller design, see Section 2.2 above, since the additional dynamics limits the overall controller performance.

2.4 Modal Identification

An extensive structural identification campaign was performed in wind-off conditions, with the wing mounted on the wind tunnel mount, see Figure 9 below. Thus, good experimental data was available both for the validation of the FE model and for the control design. For the vibration test, the model was equipped with some additional sensors to improve the quality of the identification and to validate the functionality of the internal accelerometers. In full, ten PCB 352C22 accelerometers in z-direction (vertical) and two in x-direction (in-plane) were available, a Kistler 9722A500 impact hammer was used, with no additional mass and a soft tip. Four excitation position, marked by the black arrows in Figure 8 were applied.

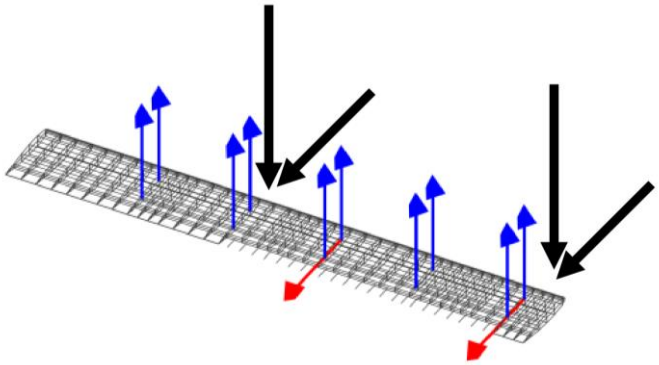

Figure 8: Sensors and excitation positions for the structural identification

For the final equipped model the following frequencies were identified:

1st wing bending	6.9 Hz
1st inplane	26.8 Hz
2nd wing bending	39.0 Hz
1st wing torsion	75.2 Hz

The finite element values match the experimental results very well for bending, but were about 20% off for torsion. The measured values were thus the basis for updating of the finite element model, see [11].

3 WIND TUNNEL TEST SETUP AND RESULTS

3.1 Wind Tunnel Setup

The wind tunnel tests were conducted in the Crosswind Simulation Facility (Seitenwindkanal Göttingen, SWG) of the German Aerospace Center (DLR) in Göttingen, which is a closed-circuit low-speed wind tunnel with a maximum flow velocity of 65 m/s, operating at ambient pressure. The dimension of the test section is 2.4 m (width) by 1.6 m (height).

The wing was mounted on an electric pitch mechanism, consisting of a servomotor and a transmission system, for both adjustment of the angle of attack and unsteady pitch excitation, see Figure 9.

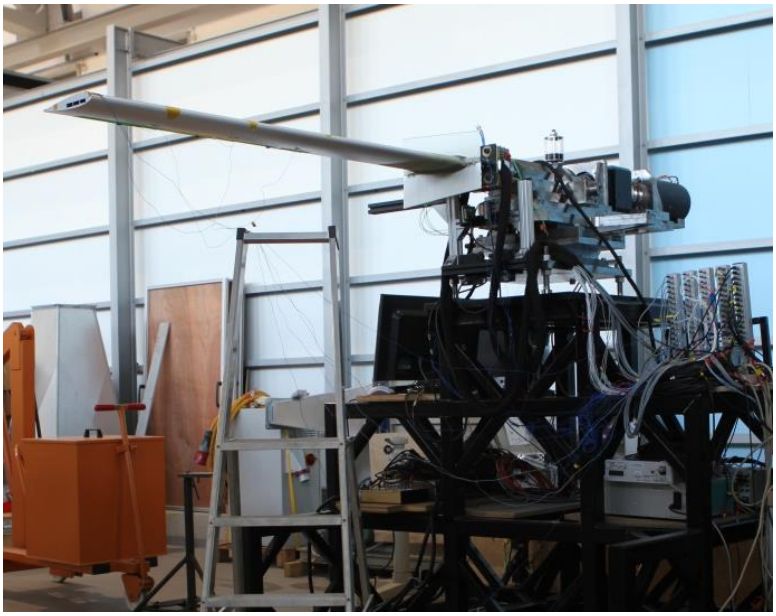

Figure 9: Wing assembly before wind tunnel testing

Steady tests were performed with flow velocities in the range of 10, 20, 30, 40, and 50 m/s. Since for flow wind speeds the aerodynamic damping increased, the controller performance could be shown best for relatively low speeds.

As the wind tunnel does not have a classical gust generator in the flow, unsteady excitation was introduced by forced rigid-body pitch motion at the wing root. The pitch motion can have and arbitrary shape, excitation signals included sine sweeps, 1-cos-inputs as well as stochastic excitations.

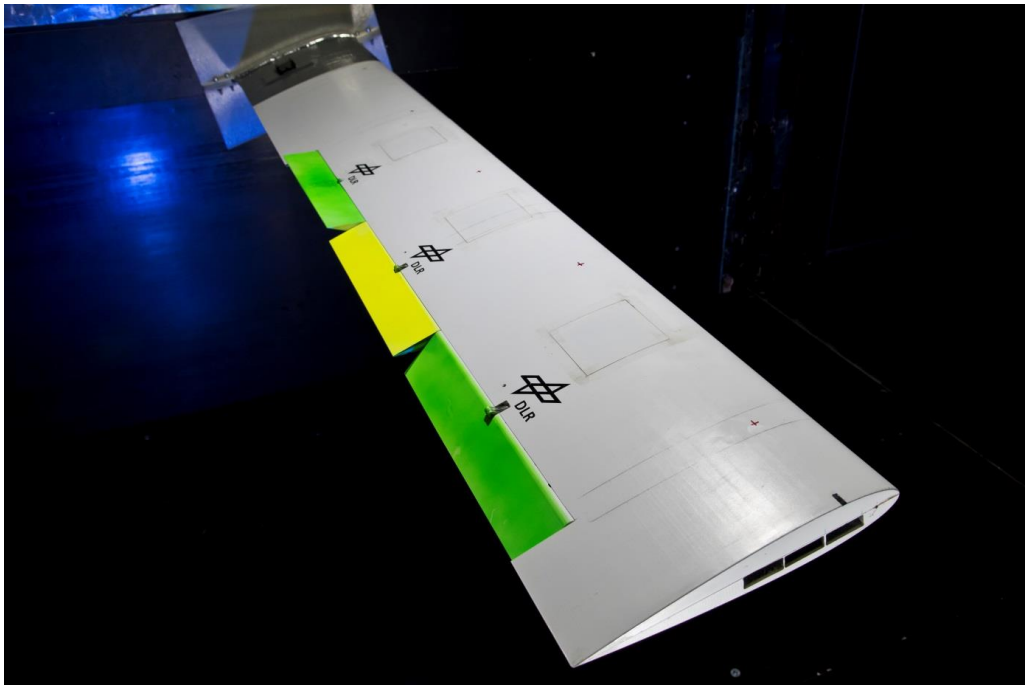

Figure 10: Wing in wind tunnel

A data acquisition system from Dewetron is used, which consists of a measuring computer and exchangeable and expandable 24-bit Delta Sigma A/D converter modules with 128 channels each, which are synchronously sampled. In addition to controlling the data acquisition, the associated software also enables the monitoring of selected sensor signals with up to 10^5 samples per second. To record the signals of the 97 sensors used and a further 41 math channels, as well as a connected camera for model observation, a sampling rate of 10^3 samples per second is selected in this test campaign. In addition, the DAQ system's internal signal generator enables the generation of a large number of analog output signals for controlling the flap and pitch movement.

The pitch oscillation test bench used consists of the Parker ST190M electric motor, whose position is controlled by a Compax3 controller, an ADwin Pro II real-time computer, and a test bench interface computer with NI LabVIEW software to adjust the model angle of attack, pitch oscillation and the wing root gust excitation, Figure 11.

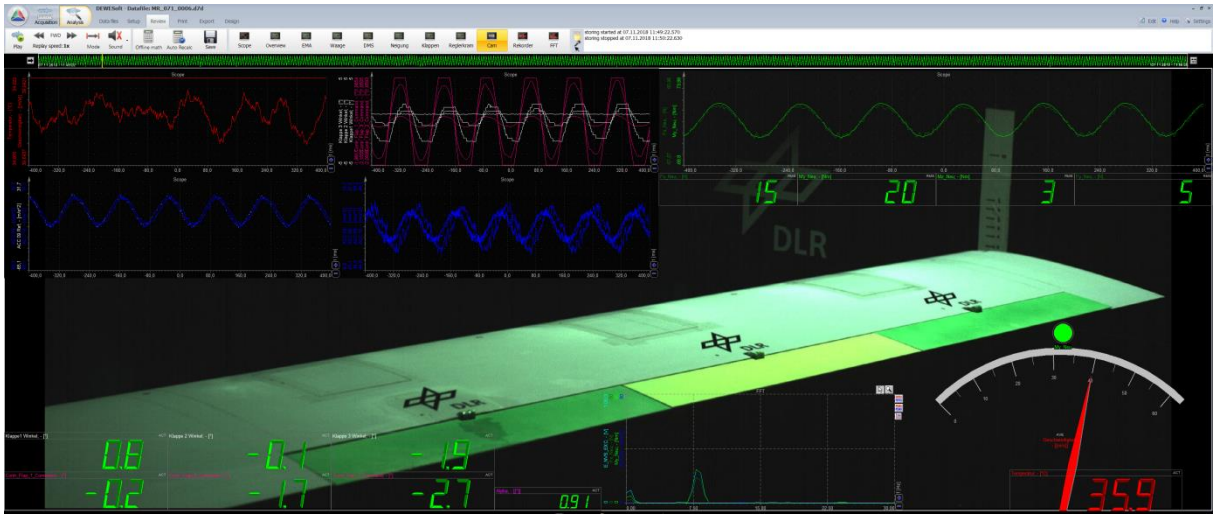

Figure 11: Data acquisition and control

3.2 Identification of Aeroelastic Model

During the test campaign Online Monitoring (OLM) was used to identify and track the modal parameters in real time. The OLM toolbox was developed in house by the Department of Structural Dynamics and System Identification at DLR Göttingen. The toolbox uses Object-Oriented Programming (OOP) with optimized methods for fast processing and visualization of big data sets. For modal analysis the data was first decimated using a Chebyshev Type I lowpass filter to a bandwidth of 250 Hz. The resulting time data from the 12 internal PCB 352C22 accelerometers measured over 5 minutes during run MR_002_0001 is shown in Figure 12. During this run the wind speed was kept constant at 40 m/s and the wing was not excited additionally by the test rig.

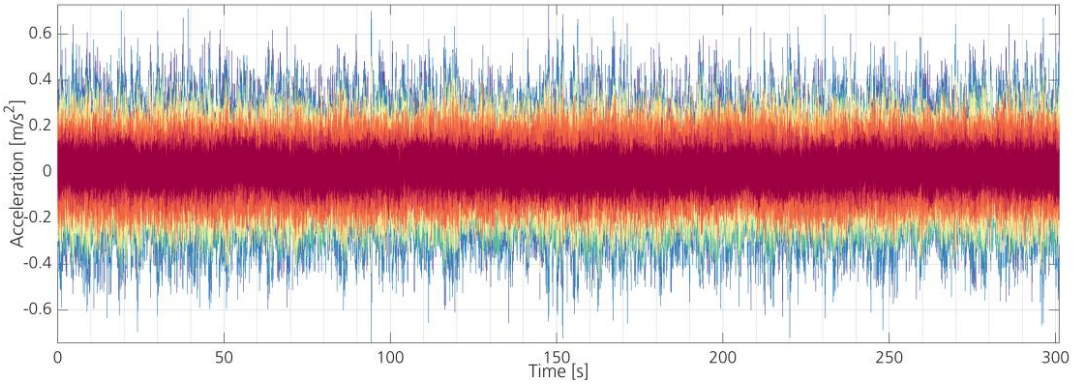

Figure 12: Time history from internal sensors during run MR_002_0001

The Auto Power Spectral Densities (APSDs) computed using a Hanning window with 66 % overlap is shown in Figure 13. It can be seen that the data contains a significant amount of noise, with distinct harmonics of the 50 Hz electrical noise. Nevertheless, several modes can also be identified visually from the spectra with different response amplitudes and levels of damping, which is indicated by the steepness of the peaks.

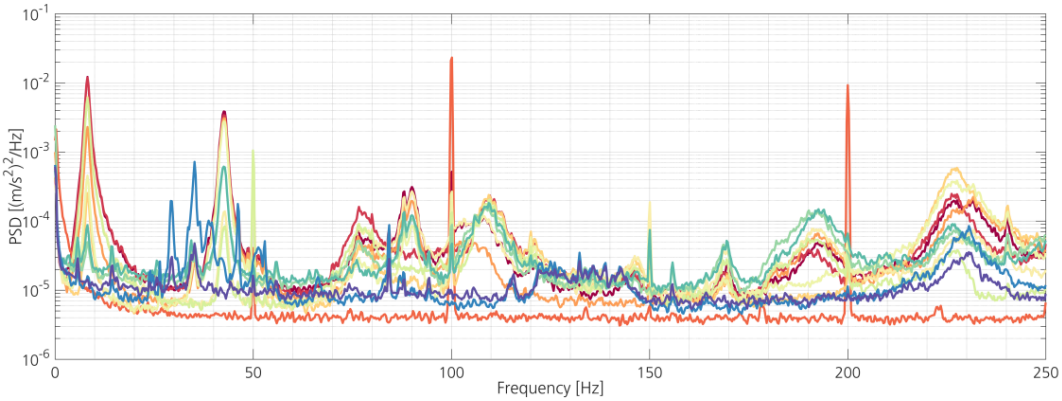

Figure 13: Auto Power Spectral Densities (APSDs)

System identification was subsequently performed on the time data using the data driven Stochastic Subspace Identification (SSI) method with a Hankel block size of 30 and model order of 80. The resulting stabilization diagram is shown in Figure 14. The respective Eigenfrequencies are shown above the bottom axis, and the Breitbach Mode Indicator Function (MIF) values above the top line for the highest model orders. The MIF provides an indicator of the mode quality regarding the complexity of the mode shape, with 1000 indicating a real normal mode. It can be observed that 13 modes are identified in the band 0

Hz to 250 Hz. Several of these modes are however spurious which are easily identified and removed by the unrealistically low damping values shown below the top line of the figure. Furthermore the SSI method has been shown to deliver unbiased estimates despite closely spaced harmonic contamination [15]. The physical modes can be seen to all have MIF over 800.

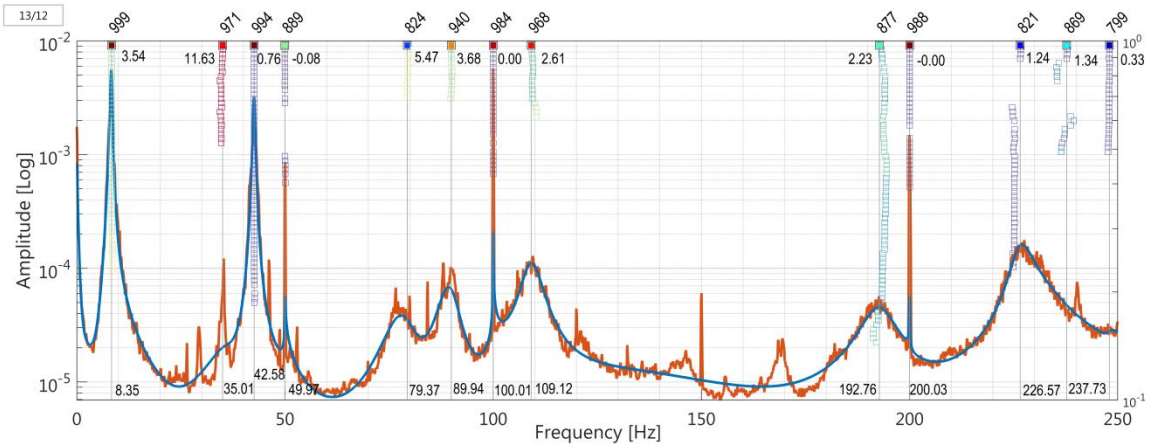

Figure 14: SSI Data Stabilization diagram

The mode shapes of the first six physical modes are shown in Figure 15. The first normal bending mode (mode #1) is identified at 8,35 Hz with damping 3,54 %, and the first inplane bending mode (mode #2) is identified at 35,01 Hz with 11,63 % damping. The second normal bending mode (mode #3) is identified at 42,58 Hz with 0,76 % damping and the first torsion mode (mode #4) is then seen 79,37 Hz with 5,47 % damping. The differences observed between the results from the hammer test and the wind tunnel excitation are due to the aerodynamic loading on the wing.

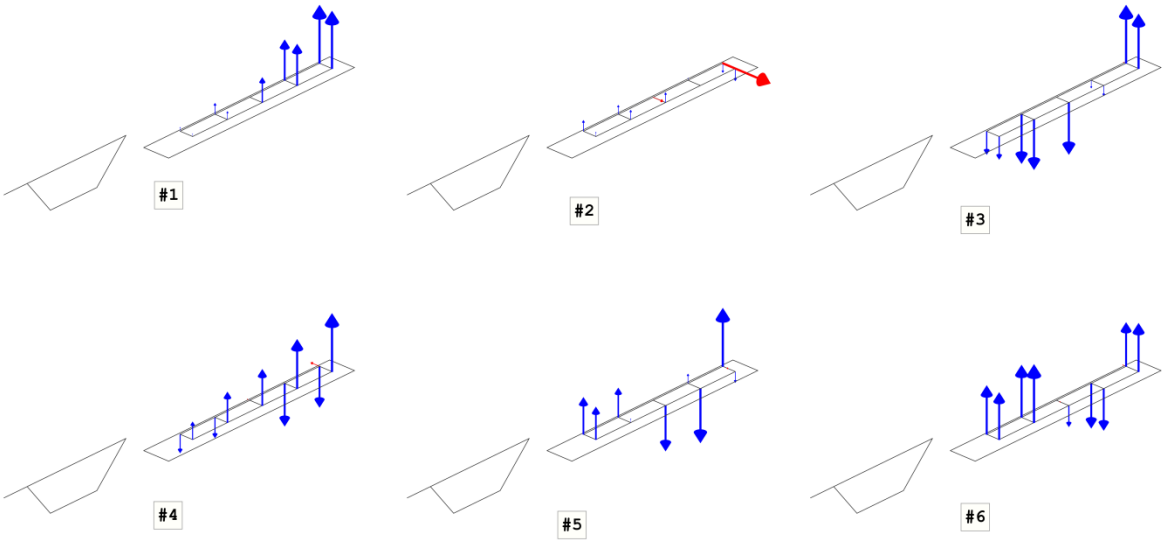

Figure 15: First six mode shapes

The results from the OLM provide valuable insight in real time into the effect of the wind speed as well as the active controller effects on the modal parameters. Furthermore the tool provides the possibility to safely push the test envelope in order to explore the boundaries of the load reduction system.

3.3 Dynamic Load Control

One main objective of the wind tunnel campaign was to assess the performance of the load control algorithm described in Section 2.2. In a first step, experimental data for the control surface aerodynamics was obtained, as a good model of control surface efficiency is is essential for successful load control. Lift polars were taken for various combinations of flap settings for a range of flow speeds.

Second, the basic load control approach was evaluated by recording the transfer function of vertical acceleration at the wing tip as a function of pitch input at the wing root. Pitch excitation under wind condition, 40 m/s, was measured in open loop and closed loop condition. The performance of the controller was assessed using these transfer functions, because the damping of the first bending mode must increase when the control is active. Figure 16 shows the transfer function of an accelerometer mounted at the tip for pitch input at wing root for the passive wing (blue) and the actively controlled wing (red). It can be clearly seen that the damping is increasing when the controller is turned on.

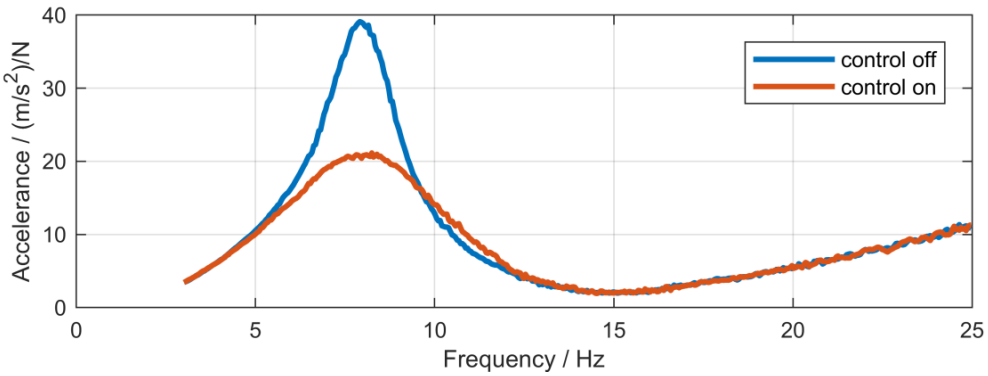

Figure 16: Transfer function of vertical acceleration at wing tip for pitch input at wing root

In order to verify the GLA capability of the controller derived in Section III, the flexible wing is excited by stochastic and discrete gusts. In the stochastic case, a band-limited noise between 1-30 Hz is commanded to the pitch excitation system. The intensity of the noise is chosen such that a maximum wing root bending moment of 120 N m is not exceeded and hence varies with airspeed. The root mean square (RMS) of the wing root bending moment is reduced by 28 % at V = 40 m/s while at V = 20 m/s, a reduction of only 10 % is achieved since flap efficiency is decreased at low airspeeds.

As discrete gust excitations, "1-cos" gusts according to the certification requirements [22] and [23] were applied. Different intensities and gust gradient distances were tested, where the wing root bending moment becomes a maximum when the gust frequency coincides with the natural frequency of the first wing bending mode. Plotting the wing root bending moment for this special case in Figure 17, it can be seen that both the peak and the settling time are reduced considerably when the controller is turned on (closed-loop). The corresponding flap deflection commands are depicted in Figure 18, where it can be seen that the outer flap is deflected most. In comparison to that, the inner flap deflection commands are within free play meaning that in reality, the inner flap is not deflected. Obviously, this yields a loss in GLA performance which is confirmed in nonlinear simulations.

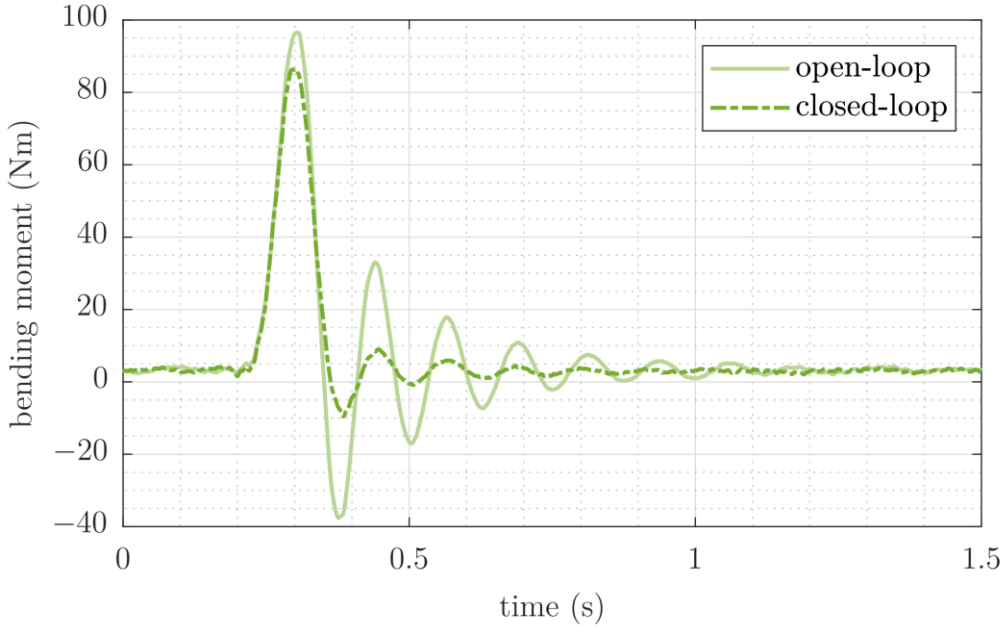

Figure 17: Comparison of wing root bending moment for "1-cos" gust excitation at V = 40 m/s with and without GLA

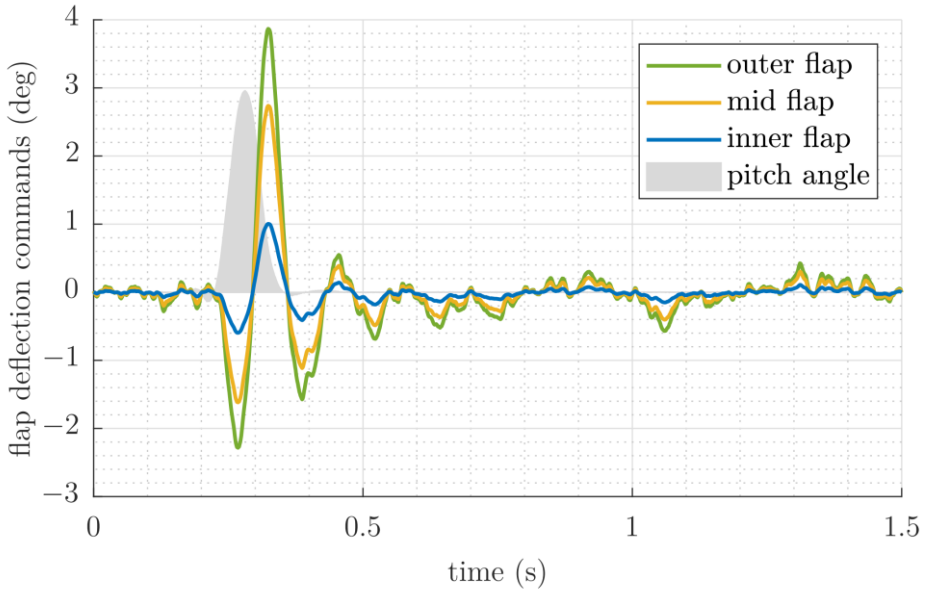

Figure 18: Flap deflection commands for "1-cos" gust excitation at V = 40 m/s

Finally, the evaluation of the control performance for a load reduction in the presence of a jammed flap was performed. Figure 19 shows the corresponding results. In the lower diagram, the root bending moment measured by the piezo balance is shown. In the upper diagram, the deflections of the three flaps are displayed in yellow, red and blue, respectively. In the first phase (“OL”, from 0 to 2 seconds), the wing was excited with no load control activated. In the second phase (“CL (nominal)”, from 2 to 4.1 seconds), the load control works with all flaps active. A peak reduction of 50 % root bending moment is realized by the control. In the third phase (“CL (fault)”, from 4.1 to 6.2 seconds), a fault is simulated by switching off the outer aileron. With only two flaps active in the same control mode as before, the root bending goes up to 75 % of the original, passive value. In the last phase (“CL (allocation)”, from 6.2 to 8

seconds), the performance of phase two (CL nominal) is reached again by re-allocating control authority to the two remaining flaps.

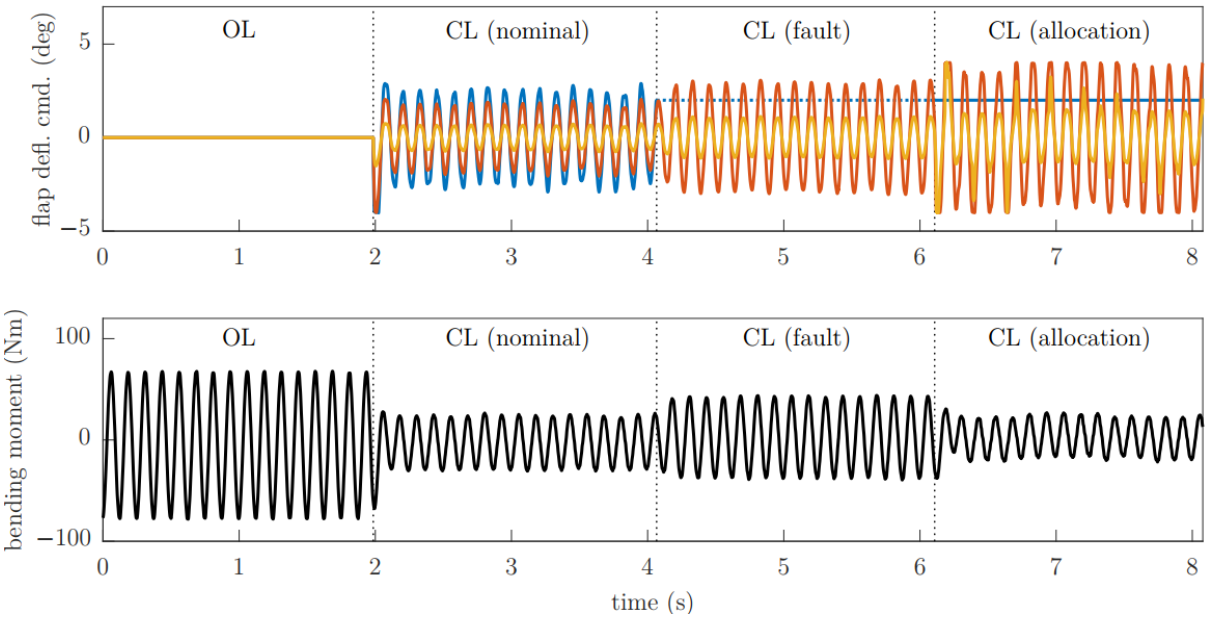

Figure 19: Deflection commands of inner (yellow), mid (red) and outer (blue) flap and the resulting wing root bending moment for the open-loop (OL) and closed-loop (CL) cases

A curious result is that the bending moment becomes smaller in the allocated case, with only two actuators operating, than in the nominal case with all three actuators working. After some closer investigation it was found that this seems to be due to the large unpredicted free-play in the inner actuator already mentioned for the “1-cos”-gust case above. In the nominal case, the control commands to the inner actuator remain largely inside the free-play area, thus reducing the potential load reduction for that operating point. When re-allocating the control authority, the inner actuator operates with larger deflections, mainly outside the free-play area, thus with the expected efficiency.

4 CONCLUSION AND OUTLOOK

With the wing design and the wind tunnel campaign, the main goals of the project could be fulfilled. The structural model was thoroughly identified, and the results served as a validation for the model. It could be shown that controller was well able to reduce the loads at the wing root, and different controller settings could be tested for a variety of excitations. Finally, the online-identification provided valuable data during the test.

Research on active low speed wind tunnel models will continue. It is planned to test the wing in a wind tunnel with a gust generator. Reduction of free-play will be a topic of concern. Another experiment in a transonic wind tunnel with a new tailored wing is planned. However, as the wing needs to be smaller due to a lower wind tunnel cross section, and because of the resulting higher reduced frequencies, an actuation via a flap is currently unrealistic.

5 BIBLIOGRAPHY

[1] W.R. Krüger, J. Dillinger, R. De Breuker, K. Haydn (2019): Investigations of Passive Wing Technologies for Loads Reduction. CEAS Aeronautical Journal, accepted for publication Apr. 2019, DOI: 10.1007/s13272-019-00393-2.

[2] W. R. Krüger, P. D. Ciampa, M. Geier, T. Kier, T. Klimmek, D. Kohlgrüber, P. Ohme, K. Risse, J. Schwinn (2018): A Comprehensive Load Process at the DLR – Definition, Analysis, and Experimental Evaluation. AerospaceLab Journal, Issue 14, Sep. 2018, DOI: 10.12762/2018.AL14-01

[3] M. Böswald, J. Schwochow, G. Jelicic, Y. Govers (2017): New Concepts for Ground and Flight Vibration Testing of Aircraft based on Output-Only Modal Analysis. In: Proc. 7th International Operational Modal Analysis Conference (IOMAC), pp. 15-34. 10.-12. Mai 2017, Ingolstadt, Germany, Shaker Verlag.

[4] H. Mai, J. Neumann, H. Hennings (2011): Gust response: a validation experiment and preliminary numerical simulations. In: Proc. IFASD 2011 - 15th International Forum on Aeroelasticity and Structural Dynamics, 27 - 30 June 2011, Paris, France. https://elib.dlr.de/70264/1/H._Mai_%2B_J._Neumann_%2B_H._Hennings.pdf

[5] T. M. Kier (2013): An Integrated Loads Analysis Model for Wakevortex Encounters. Proc. IFASD 2013 - International Forum on Aeroelasticity and Structural Dynamics, 24–27 June 2013, Bristol, UK.

[6] C. Weiser, D. Ossmann, R. Kuchar, G. Looye (2019): Design and Verification of a Linear Parameter Varying Control Law for a Transport Aircraft. 5th CEAS Specialist Conference on Guidance, Navigation & Control (EuroGNC), 03. - 05. Apr. 2019, Mailand, Italien.

[7] M. Pusch (2018): Aeroelastic Mode Control using H2-optimal Blends for Inputs and Outputs. In Proc. 2018 AIAA Guidance, Navigation, and Control Conference, 8–12 January 2018, Kissimmee, Florida.

[8] M. Y. Meddaikar, J. Dillinger, J. Sodja, H. Mai, R. De Breuker (2016): Optimization, Manufacturing and Testing of a Composite Wing with Maximized Tip Deflection. In: Proc. 57th AIAA/ASCE/AHS/ASC Structures, Structural Dynamics, and Materials Conference. AIAA SciTech Forum, 4-8 Jan 2016, San Diego, USA. DOI: https://doi.org/10.2514/6.2016-0489 ISBN 978-1-62410-392-6

[9] M. Y. Meddaikar, J. Dillinger, M. R. Ritter, Y. Govers (2017): Optimization & Testing of Aeroelastically-Tailored Forward Swept Wings. Proc. IFASD 2017 - International Forum on Aeroelasticity and Structural Dynamics, Como, Italy, 2017.

[10] J. Dillinger (2014): Static Aeroelastic Optimization of Composite Wings with Variable Stiffness Laminates. Dissertation, Delft University of Technology, 2014.

[11] J. K.S. Dillinger, Y. M. Meddaikar, J. Lübker, M. Pusch, T. Kier (2019): Design and Optimization of an Aeroservoelastic Wind Tunnel Model. International Forum on Aeroelasticity and Structural Dynamics, Savannah, Georgia, USA, 2019.

[12] D. Ossmann, M. Pusch (2019): Fault Tolerant Control of an Experimental Flexible Wing. Submitted to Aerospace Journal, MDPI, 2019.

[13] M. Pusch, D. Ossmann, J. Dillinger, T. M. Kier, M. Tang, and J. Lübker (2019): Aeroelastic modeling and control of an experimental flexible wing. Proc. 2019 AIAA Guidance, Navigation, and Control Conference, AIAA SciTech Forum, San Diego, USA, 2019.

[14] C. D. Regan (2017): mAEWing2: Conceptual Design and System Test. Proc. AIAA Atmospheric Flight Mechanics Conference, (SciTech) January 2017. DOI: 10.2514/6.2017-1391.

[15] K. Soal (2018): System Identification and Modal Tracking on Ship Structures. PhD Thesis. Stellenbosch University.